

# **HHS Public Access**

Author manuscript

Curr Biol. Author manuscript; available in PMC 2020 June 17.

Published in final edited form as:

Curr Biol. 2019 June 17; 29(12): 2083-2090.e4. doi:10.1016/j.cub.2019.05.034.

# Retrosplenial cortical representations of space and future goal locations develop with learning.

Adam M. P. Miller<sup>1</sup>, William Mau<sup>2</sup>, and David M. Smith<sup>1</sup>

<sup>1</sup>Department of Psychology, Cornell University, Ithaca, NY 14853

<sup>2</sup>Center for Memory and Brain, Boston University, Boston, MA 02215

# **Summary**

Recent findings suggest that long-term spatial and contextual memories depend on the retrosplenial cortex (RSC) [1-5]. RSC damage impairs navigation in humans and rodents [6-8] and the RSC is closely interconnected with brain regions known to play a role in navigation, including the hippocampus and anterior thalamus [9, 10]. Navigation related neural activity is seen in humans [11] and rodents, including spatially localized firing [12, 13] and directional firing [12, 14, 15], and responses to navigational cues [16]. RSC neuronal activity is modulated by allocentric, egocentric, and route-centered spatial reference frames [17, 18], consistent with an RSC role in integrating different kinds of navigational information [19]. However, the relationship between RSC firing patterns and spatial memory remains largely unexplored, as previous physiology studies have not employed behavioral tasks with a clear memory demand. To address this, we trained rats on a continuous T-maze alternation task and examined RSC firing patterns throughout learning. We found that the RSC developed a distributed population-level representation of the rat's spatial location and current trajectory to the goal as the rats learned. After the rats reached peak performance, RSC firing patterns began to represent the upcoming goal location as the rats approached the choice point. These neural simulations of the goal emerged at the same time that lesions impaired alternation performance, suggesting that the RSC gradually acquired task representations that contribute to navigational decision-making.

#### eTOC Blurb

Miller *et al.* find that spatial representations develop in the retrosplenial cortex (RSC) as rats learn a memory guided spatial navigation task. Spatial information is encoded in the form of population firing patterns and, after learning, these firing patterns simulate future goal locations, suggesting an RSC role in navigational planning.

**Lead Contact:** Adam M. P. Miller, Cornell University, Department of Psychology, B59 Uris Hall, Ithaca, NY 14853, 647-901-2676, amm473@cornell.edu.

Author Contributions

A.M.P.M. and D.M.S. designed the experiments and wrote the paper. A.M.P.M. and W.M. conducted the experiments. A.M.P.M. performed the analyses.

**Publisher's Disclaimer:** This is a PDF file of an unedited manuscript that has been accepted for publication. As a service to our customers we are providing this early version of the manuscript. The manuscript will undergo copyediting, typesetting, and review of the resulting proof before it is published in its final citable form. Please note that during the production process errors may be discovered which could affect the content, and all legal disclaimers that apply to the journal pertain.

Declaration of Interests

The authors declare no competing interests.

#### **Keywords**

Memory; Cingulate; Long-term; Consolidation; Prediction; Decision making; Attention; Simulation; Space; Navigation

#### Results

#### RSC neural populations develop a representation of the maze with learning

We recorded neuronal firing in the RSC (Figure S1A) as rats learned and performed a continuous alternation task (Figures 1A and 1B) and we focused our analyses on four training stages: early, middle, and late learning, as well as asymptotic performance sessions (see STAR Methods). Consistent with previous reports [13, 17, 18, 20], RSC neurons exhibited broad firing fields with high background firing rates, unlike hippocampal place cells. However, the firing rate differences across broad regions of the maze were quite reliable (Figure 1C), resulting in a representation of the maze that could be seen at the population level. This representation improved with learning. We used Bayesian decoding to predict the rat's current location on the basis of firing patterns from simultaneously recorded RSC populations [21, 22] (Figure 1D; Figures S2A–C) and found that the rat's location could be predicted at a rate far greater than chance, even during earliest stages of learning (p < 0.001, compared to a shuffled control distribution, see STAR Methods; Figure 1E), and that decoding accuracy improved significantly as the rats learned (F(3,30) = 4.08, p < 0.05). At asymptote, the position of the rat on the maze could be accurately predicted within 4.5 cm about 40% of the time.

We confirmed this result with correlational reconstruction analysis by combining neurons from all rats into a single population vector for each training stage, calculating mean firing rate vectors for each spatial bin separately for the first and second halves of the session, and then correlating those vectors. The resulting correlation matrices reflect the similarity of spatial firing patterns across the session halves (Figure 1F). If spatial firing is reliable the highest correlation should occur between visits to the same location, along the diagonal, while deviations from the diagonal indicate instances of unreliable spatial coding (i.e. spatial coding errors). Consistent with the Bayesian analysis above, spatial coding was far more reliable and accurate than expected by chance at all stages of learning (all p < 0.001, compared to a shuffled control distribution) and the representation improved with learning, as indicated by a 64% reduction in spatial coding errors from early learning to asymptotic performance (p < 0.005, compared to a shuffled control distribution; Figure 1G).

Spatial representations were observed despite the fact that individual RSC neurons exhibited relatively non-specific firing fields. As with other neocortical systems [23, 24], RSC spatial representations took the form of a distributed population code in which individual neurons contribute a small amount of information and precision is only achieved at the population level (Figure S2). The observation that these representations improved with learning raises the question of how the firing characteristics of the constituent neurons changed to support the improved population representations. Individual neurons did not acquire more hippocampus-like place fields, but instead the broad firing patterns across maze regions

became more reliable with learning and the reliability of spatial firing was specifically associated with learning rather than mere exposure to the maze (Figures S2L and S2M).

Mazes necessarily constrain subjects' behavior and RSC neurons are sensitive to behavioral variables such as running speed, head direction and turns [17, 18]. However, the quality of spatial representations was not associated with running speed (Figures S3D–F) and few neurons exhibited strong directional or turn-related firing (Figures S3K–M). Nearly all neurons exhibited spatial firing that could not be attributed to movement variables (Figure S3M). For our analysis of learning related changes in RSC representations, we limited our analysis to trials with consistent running behavior to ensure that representational changes were not due to changes in running speed or behavioral consistency (Figures S3B and S3C).

### RSC neural populations develop trial-type specific responses on the stem of the maze

RSC neurons exhibited differential firing on the stem of the maze depending on whether the rat subsequently made a left or right turn at the choice point, similar to previous reports from the hippocampus [25] (Figure 2A). This trial-type specific firing increased with learning to include 21% of neurons at asymptote, which was significantly greater than chance (p < 0.001, compared to a shuffled control distribution), and this increase was also seen across neuronal populations from individual rats (F(3,35) = 5.80, p < 0.01; Figure 2B). These firing patterns were not caused by differences in the rat's head direction or trajectory (Figures S3G–J). We also assessed trial-type specificity at the population level by combining neurons from all rats into a single population vector for each trial and computing the distance to other left and right trials. The firing patterns became more trial-type specific with learning (F(3,100) = 20.02, p < 0.001, Figures 2C and 2D), indicating that activity on left trials became more similar to other left trials, and less similar to right trials (and likewise with right trials). Stem firing patterns were sufficiently distinct that we could use a linear classifier to predict the upcoming left or right turn on the basis of the firing patterns. Prediction accuracy increased with learning (p < 0.05, compared to a shuffled control distribution, Figure 2E), from chance levels early in learning to perfect accuracy during asymptotic performance. Interestingly, stem firing patterns were also related to alternation accuracy. We binned asymptotic performance sessions into four categories based on overall performance, and found that sessions with better alternation accuracy had higher neural trialtype specificity (F(3, 132) = 24.38, p < 0.001; Figures 2F and 2G). Similarly, our ability to predict left or right turns on the basis of stem firing patterns was better on superior performance days than on poor performance days (p < 0.05, compared to a shuffled control distribution, Figure 2H).

#### RSC populations represent future goal locations

The RSC is active during route planning in humans [11] and RSC neurons encode goal locations in rodents [16], suggesting that RSC neurons might represent future goal locations as reported in the hippocampus and striatum [26, 27]. After confirming that RSC population activity distinguished the two reward locations in this task (Figure S2J; see also [16]), we used Bayesian decoding to determine whether RSC activity represented the distant reward locations as the rats traversed the stem toward the choice point (Figure 3). This involves computing the probability of finding the rat at every maze location given the instantaneous

population activity. Individual examples of instantaneous decoding are shown in Figure 3A. The average of all decoded instances is shown for each training stage in Figure 3C, which illustrates the total amount of decoding observed at every maze location, including all the population data from all subjects. As expected, most of the decoding indicated the rat's current position on the stem of the maze. However, substantial and selective decoding to the distant reward areas is also evident (arrows). Overall, 25.42% of the decoded probability distribution was located in the reward regions (boxes in Figure 3B). Decoding to the two reward areas increased with learning (F(3,30) = 3.73, P < 0.05, Figures 3C and 3D) from marginally greater than chance during the early and middle stages of learning (early,  $t_{(5)}=2.36$ , P = 0.07; middle,  $t_{(4)}=2.83$ , P = 0.05) to far greater later in learning (late,  $t_{(7)}=5.14$ , P < 0.005; asymptote,  $t_{(14)}=9.56$ , P < 0.001).

RSC populations initially represented both the correct and incorrect reward areas equally. However, they began to preferentially represent the correct reward area after the rats became proficient at the task. To quantify this, we compared the decoded probability in the correct reward area, p(correct), with the opposite reward area, p(incorrect, Figure 3B), and found that RSC populations increasingly represented the correct future reward area rather than the incorrect area with learning (F(3,30) = 10.28, p < 0.001, Figures 3C and 3E). Although RSC populations showed an apparent preference for the incorrect (previously visited) reward area early in learning, after correcting for multiple comparisons preferential decoding to a specific reward location was only significant during asymptotic performance sessions  $(t_{(14)} = 3.48, p < 0.005)$ . Preferential decoding to the correct reward area was not attributable to behavioral factors such as head direction (Figures S3I and S3J).

Selective representations of the future goal location only emerged during asymptotic performance and some studies indicate that RSC lesions selectively impair performance at asymptote [28, 29]. To examine this, we made neurotoxic (NMDA) lesions of the RSC in a separate group of rats and trained them on the continuous alternation task. The early stages of learning were not affected by the lesions. However, the lesions caused a modest but reliable impairment in asymptotic performance, the same learning stage where representations of the correct goal location emerged in our neural data. A two-way repeated measures ANOVA comparing the performance of control rats and rats with lesions revealed a significant training stage by lesion group interaction ( $F_{(6,90)} = 2.832$ , p < 0.05, Figure 3F; Figure S1E). Post-hoc comparisons confirmed that the impairment was selective to asymptotic performance ( $t_{(15)} = 3.47$ , p < 0.005; Figure 3F **inset left**; Figure S1F) and tightly correlated with lesion size (r = -0.90, p < 0.01; Figure 3F **inset right**).

#### Discussion

These findings indicate that rich and detailed spatial representations develop in the RSC over the course of learning, including information about the rat's current spatial location, current trajectory, and representations of upcoming goal locations. Each of these representations emerged on its own time course. Spatial representations, like behavioral performance, were well above chance on the first day of training and they continued to improve over the course of multiple training sessions. RSC populations did not initially distinguish left and right stem traversals, but began to do so as the rats learned. Finally, selective representations of

the correct goal location only emerged after the rats reached asymptotic performance. This pattern of results is consistent with recent studies suggesting that the RSC is a key component of the neocortical system for storing long-term spatial memory [2–5, 30].

The RSC encoded the rat's current spatial position, but it also generated more complex representations that may be important for goal directed navigation and planning. Previous studies have shown that RSC firing is sensitive to the sequences of turns that define a trajectory [17, 18], and the trial-type specific firing we observed here may reflect distinct RSC representations of the separate trajectories to the goal locations, left-to-right and rightto-left, which share the stem as a common segment. This is consistent with numerous reports of trajectory specific firing in the hippocampus [25, 31]. Goal locations are a prominently represented in the RSC [16] and we found that RSC populations transiently represented the distant goal location as the rats approached the choice point. Similar representations have been observed in the hippocampus and the ventral striatum, where simulations took the form of sequential reactivation of neurons encoding locations along the path to the goal [26] and reactivation of reward-encoding neurons [27], respectively. Our data contain elements of each of these findings, with RSC populations sometimes reactivating spatial firing patterns that corresponded to positions on approach to the reward but most frequently corresponding to the reward location itself (Figure 3C). We did not see clear evidence of forward sweeping simulations of the path to the reward.

This provides an interesting, if speculative, convergence with human studies of the default mode network, which includes the RSC, prefrontal cortex, posterior parietal cortex and hippocampus, and is thought to mediate constructive memory processes that underlie both episodic memory and the ability to imagine future events [32, 33]. Many of these regions are also involved in route planning in humans [11, 34], and evidence for representations of future routes and goal locations has been reported in several of these regions in rats [35–37]. The relatively simple future reward simulations seen in rodents may be the rudimentary building blocks for the complex future simulation abilities of humans [38, 39]. In our data, representations of the correct goal location only emerged during asymptotic performance, after other RSC spatial representations had formed. Together with our finding that RSC lesions selectively impaired performance at asymptote, these data suggest that future reward representations may contribute to route planning, but only after other spatial representations, such as map-like representations of the maze, have become sufficiently stable.

The mechanisms that drive the learning related development of RSC spatial representations are not known. However, the functional similarities and anatomical connectivity with the hippocampus [40] suggest that the emergence of RSC representations may reflect consolidation of information from the hippocampus [41]. Consistent with this idea, contextual fear memories depend on the hippocampus early after learning but later become more reliant on the RSC [2, 42]. In a striking example, optogenetic reactivation of an RSC context representation was sufficient to evoke a contextual fear memory, even when the hippocampus was inactivated [3], and reactivation of the RSC representation during sleep reduced the importance of the hippocampus for retrieval [4]. Recent in vivo imaging studies have found that RSC neurons exhibit sequential firing on a treadmill task but the emergence

of these patterns is blocked by hippocampal lesions [43], and spatial learning recruits RSC populations that remain stable for weeks [5]. Several of our observations are suggestive of a distributed cortical representation resulting from systems consolidation [41]. RSC lesions had no effect on the early stages of learning and only impaired performance after the task was well learned. Moreover, the lesion-induced performance deficit, though modest, was tightly correlated with the amount of tissue damage and spatial representations were spread across a large cortical region consistent with a distributed representation. The representations that support spatial navigation likely extend to other midline cortical regions such as the anterior cingulate [44] and prefrontal cortex [35] and these regions may support the relatively good performance seen in subjects with RSC lesions. However, the complex spatial representations of the RSC have not been observed in other cortical regions [35], suggesting that examination of the RSC and its interactions with the hippocampus will be particularly important for understanding spatial memory.

#### **STAR Methods**

#### CONTACT FOR REAGENT AND RESOURCE SHARING

Further information and requests for resources and reagents should be directed to and will be fulfilled by the Lead Contact, Adam M. P. Miller (amm473@cornell.edu).

#### **EXPERMENTAL MODEL AND SUBJECTS DETAILS**

**Subjects**—Subjects were 32 adult male Long Evans rats (Charles River Laboratories, Wilmington, MA) weighing 250g-300g upon arrival. Twelve rats were used in the neurophysiology study and 20 rats were used in the lesion study. Rats were randomly assigned to control and lesions conditions. Of the 10 rats that received RSC lesions, 2 were excluded from the analysis due to hippocampal damage, and 1 was excluded because the RSC damage was unilateral. Rats were placed on a 12hr/12hr light/dark cycle with lights on at 8am and allowed to acclimate to the vivarium for at least one week prior to surgery. After recovery from surgery, rats were placed on food restriction until they reached 80-85% of their free-feeding weight. Water was always available ad libitum. All procedures complied with the guidelines of the Cornell University Animal Care and Use Committee.

#### **METHOD DETAILS**

**Surgery—**For the neurophysiological recording study, fifteen rats had a custom-built electrode microdrive implanted, which contained 20 moveable tetrodes (16 recording tetrodes and 4 reference tetrodes) made from twisting four 17μm platinum/iridium (90%/ 10%) wires, platinum plated to an impedance of 100-500 kΩ, and arranged in two 10-tetrode linear arrays (one in each hemisphere) that spanned approximately 5mm along the rostrocaudal axis of the brain. Tetrodes were stereotaxically positioned bilaterally just beneath the cortical surface (2-7 mm posterior to Bregma,  $\pm 1.5$ mm lateral) with the tetrodes angled 30 degrees toward the midline. Rats were given 7 days to recover from surgery prior to lowering the tetrodes into the RSC (35-70 μm daily) over the course of several days until a depth of at least 1 mm was reached to ensure that the tetrodes were in the granular b subregion (discussed below).

For the lesion experiment, twenty rats were anesthetized with isoflurane gas (1-5% in oxygen) and placed in a Kopf stereotaxic apparatus. The skin was retracted and holes were drilled through the skull above each of the injection sites. Ten rats received bilateral neurotoxic (N-methyl-D-aspartate [NMDA],  $10\mu g/ml$ ) lesions of the RSC. NMDA was injected by hand in volumes of  $0.20-0.35~\mu l$  using a custom-made glass injection canula (100 $\mu m$  diameter) attached to a Hamilton Syringe by sterile plastic tubing. The stereotaxic coordinates and injection volumes were:

- 1.  $0.35\mu L$  at -2.2 (AP),  $\pm 0.5$  (ML), -3.0 (DV)
- 2.  $0.35\mu L$  at -3.9 (AP),  $\pm 0.5$  (ML), -3.0 (DV)
- 3.  $0.20\mu L$  at -5.5 (AP),  $\pm 0.5$  (ML), -3.5 (DV)
- 4.  $0.35\mu L$  at -5.5 (AP),  $\pm 1.0$  (ML), -2.8 (DV)
- 5.  $0.35\mu L$  at -6.7 (AP),  $\pm 1.1$  (ML), -2.8 (DV)
- 6.  $0.30\mu L$  at -8.0 (AP),  $\pm 1.3$  (ML), -2.8 (DV)

Coordinates were taken from Bregma (AP), the midline (ML), and the surface of the skull (DV), respectively. The injection cannula was left in place 1 min before and 5 min after each infusion. An additional ten rats received sham lesions of the RSC consisting of lowering the injection cannula into the brain but not injecting NMDA.

**Continuous T-Maze Apparatus**—Rats were trained on a black PVC continuous T-maze (120 cm long stem x 100 cm wide x 68 cm above the floor) with metal reward cups embedded in the ends of the arms. Chocolate milk (0.2 ml, Nestle's Nesquik) was delivered to the reward cups via an elevated reservoir controlled by solenoid valves activated by footpedal switches. The maze was located in the center of a circular arena enclosed by black curtains with visual cues of various shapes, sizes, and colors. The room was illuminated by a ring of LED lights around the edge of the ceiling. A continuous background masking noise was played from a speaker located directly above the apparatus.

Behavioral Training Procedures—Prior to training, rats were acclimated to the maze and chocolate milk rewards with daily periods of free exploration on the maze until rats consumed 20 rewards within the first 10 min of an acclimation session (mean = 4.5 acclimation days). After acclimating to the maze, rats were trained on a continuous spatial alternation task in which the rats were rewarded only if they approached the opposite (left or right) reward location from the previous trial. Both cups were baited on the first trial. Entries into the same arm as the previous trial were scored as an error and were not rewarded. Unlike some previous studies [25], rats were not shaped with trials where the incorrect choices were prevented by blocking access. Instead, rats were gently ushered back if they left the continuous alternation route. Rats were not allowed to correct their errors. Rats were given 40 trials/day until they achieved a criterion of 90% correct on two consecutive days. After achieving this criterion, rats were given up to 10 additional training sessions to record neuronal activity during asymptotic performance. This task was selected because it has a clear memory requirement with an unambiguous measure of performance (% correct) and an

extensive body of data on spatial representations from the hippocampus and other brain regions [25, 35].

Recordings—Neuronal spike data and video data were collected throughout learning (Digital Cheetah Data Acquisition System, Neuralynx, Inc. Bozeman, MT), filtered at 600Hz and 6kHz, digitized and stored to disc along with timestamps for offline sorting (SpikeSort3D, Nueralynx, Inc.). The rat's position and head direction were monitored by digitized video of an LEDs attached to the rat's head. The time of reward receipt was measured with a grounding circuit that detected oral contact with the chocolate milk reward.

**Histology**—After completion of the experiment, rats were transcardially perfused with 4% paraformaldehyde in phosphate buffered saline. Brains were removed and stored for at least 24hrs in 4% paraformaldehyde before being transferred to a 30% sucrose solution for storage until slicing. Coronal sections (40 µm) were stained with 0.5% cresyl violet for visualization of tetrode tracks (for neurophysiology recording implants) or tissue damage (in the case of NMDA lesions). Tetrode positions were identified using depth records noted during tetrode lowering and tracks observed in the stained tissue (Figure S1A). Boundaries of the RSC were determined in accordance with The Rat Brain in Stereotaxic Coordinates [45]. Neuronal records from tetrodes located outside of the RSC were excluded from the data set. As in our previous work [16], our recordings targeted the granular b subregion of the RSC, although 31 (~4% of all recorded neurons) neurons from the dysgranular RSC were also included. For the lesion study, tissue damage was quantified by laying a grid (250 um to-scale grid spacing) over an enlarged image of the stained tissue and dividing the number of grid intersections located over damaged RSC areas by the number of intersections located over the entire RSC. No obvious relationship was seen between damage to different RSC sub-regions and alternation behavior.

#### **QUANTIFICATION AND STATISTICAL ANALYSIS**

We recorded from 637 RSC neurons in 12 rats (Figure S1A). Because representations took the form of distributed population codes, we adopted an approach of including all of the data whenever possible. We did not pre-classify neurons according to response types or exclude neurons from the analyses on the basis of their responses. However, we did exclude a small number (n=4) of clear head direction cells that produced spurious 'spatial firing' on the parts of the maze where the rat faced the relevant direction. We separated the data by subregion, hemisphere, and AP coordinates and found no conspicuous differences in the prevalence of various firing characteristics so neurons from all areas were included in the analyses. However, this does not preclude the possibility that regional differences might be found in other contexts. Rats took 4–7 training sessions to reach asymptotic performance (90% correct criterion, mean = 5.5 sessions). In order to assess changes in neuronal activity at different time points across learning, we divided the training sessions into early, middle, and late segments for analysis. We also recorded as many post-criterial asymptotic performance sessions as possible for each rat and treated these as a fourth training stage. The learning curves and grouping of sessions into training stages are illustrated in Figures S1C and S1D.

Spatial Representations.—Bayesian decoding was used to predict the current position of the rat on the maze given the spiking activity of simultaneously recorded RSC populations and a uniform prior [21] (Figure 1D). This analysis was restricted to recording sessions with at least 8 RSC neurons (34 sessions). This population size was chosen to balance the trade-off between including only the largest populations and maximizing the number of included sessions (all population sizes are shown in Figure S1D). Decoding was performed iteratively using a trial-based procedure whereby spike counts during time bins (200ms taken every 50ms) from one trial were used as the test sample, while the bins from all other trials were used as the training sample. The training sample was used to calculate firing rate maps for every neuron over a 50 X 50 grid overlaying the maze (mean of 352 visited pixels with each pixel approximately 2.5 X 2.5 cm). Probability distributions of spike counts for each neuron and pixel were computed based on the mean spike counts and assuming a Poisson distribution. For each time bin in the test sample, the probability of the rat being in a pixel was calculated by multiplying, across neurons, the conditional probabilities of observing those spike counts if the rat occupied that pixel. The highest probability pixel was taken as the decoded position of the rat on the maze, and was considered an instance of correct decoding if it was within 4.5 cm of the rat's actual head position (i.e. within a circle with a diameter of approximately the body length of a rat). Decoding accuracy was compared to a distribution of chance accuracies obtained by shuffling 10,000 times the spike counts of each neuron independently among the time bins for each recording session in that learning stage. The observed accuracy was considered significant if it was greater than 97.5% of the shuffle outcomes (2-tailed alpha of 5%).

Correlation matrices were created to quantify the selectivity and reliability of RSC spatial firing throughout learning (Figures 1F and 1G). This analysis was designed to provide a second, mathematically independent assessment of whether spatial representations improved with learning, in addition to the above-described Bayesian decoding approach. A single lap around the maze, beginning after the stem on a go-right trial and ending in the start area after a go-left trial, was divided into 170 spatial bins. Standardized mean firing rate vectors were then calculated for each spatial bin independently for the first and second half of each session (firing rate vectors contained the trial-averaged firing rate of every cell). To maximize comparability between learning stages, which had varying numbers of recorded neurons and systematic differences in behavior (i.e. more variable behavior was seen during early learning stages), the firing rate vectors were assembled from the first 50 neurons recorded during that stage and the analysis was limited to trials where the rat made typical passes through the maze section. Typical passes were defined as path lengths through a maze section that were shorter than 50% of all observed path lengths (from all rats and learning stages) through that section. This criterion was chosen because it eliminated instances where the rat's trajectory through space was interrupted by backtracking, digressions, or pauses (see Figure S3A). Sessions with fewer than five typical passes for each trial type (left and right) and session half were excluded.

Separate correlation matrices were then generated for each learning stage (early, middle, late, and asymptotic performance). Each row of a correlation matrix corresponds to the correlation of the population rate vector for one spatial bin during the first half of the session

with the population rate vectors for every spatial bin during the second half of the session. If spatial firing was perfectly reliable between the first and second halves of the session, then the highest correlation would always be between a spatial bin and itself (e.g., bin 1 in the first half of the session would be most correlated with bin 1 in the second half of the session). In this case, the diagonal from the upper left to the lower right would contain the highest r value in each row. We therefore quantified spatial coding error by computing divergence from the diagonal. Specifically, mean spatial coding error was computed by summing, over all rows, the distance between the observed maximum correlation and the diagonal, multiplying this value by the length of each bin (3cm) and then dividing by the number of bins (170). To be conservative, the maze was treated as circular for computing distance, and the shorter of the two distances (forward or backward) between the reconstructed and actual positions was always used. Higher values indicated poor spatial coding. The observed spatial coding error was compared to a chance distribution of spatial coding errors computed by shuffling the first-half second-half neuron pairings. To then determine the statistical significance of differences between training stages we compared the observed differences (in terms of mean squared error, MSE) to a distribution of differences obtained by shuffling the 200 neurons (50 per learning session) randomly between the four stages 10,000 times and each time recalculating the total spatial coding errors for each stage and the MSE between them. The observed MSE was considered significant if it was greater than 97.5% of shuffle-generated MSEs. This analysis included only a single stem traversal (from the right to left reward location) for simplicity because trial-type specific firing on left and right trials can affect the correlations. However, similar results were obtained when the stem was included twice (as two separate trajectories for left and right trials) or when the stem was excluded altogether.

Trial-type specific firing on the stem.—Individual neurons exhibiting trial-type specific firing as the rat traversed the stem were identified by comparing firing between left and right trials in each of four equal sized stem sectors (see Figures 2A and S3G) using a two-way, repeated-measures ANOVA using the same procedures as the original report of similar hippocampal firing patterns [25]. Analyses were restricted to correct trials with stem runs that did not involve pauses or deviations from smooth locomotion (i.e. typical stem runs). Typical stem runs were defined as passes through the stem of the maze that took less than 1.24s. This criterion was 2.5 standard deviations above the mean run time and eliminated trials with irregular behaviors (e.g., backtracking, digressions, or pauses), and excluded 13.77% of learning trials and 3.63% of asymptotic performance trials, see Figure S3H). To avoid comparing learning stages with different numbers of correct trials, in this analysis and all others we included only the maximum number of correct trials available for all rats (10 trials in this analysis). The statistical significance of the observed proportion of neurons was determined by shuffling 10,000 times both the (1) firing rates on each trial between the four sectors and (2) whether a trial was considered go-left or go-right, while maintaining the original proportion of each type. The observed proportion was considered significant if it was greater than 97.5% of shuffle proportions.

To assess the trial-type specificity of population firing on the stem, we combined neurons across rats and sessions to form population firing rate vectors during stem traversals on left

and right trials, and then computed a specificity measure that quantified how similar activity during each stem traversal was to other traversals of the same trial type (e.g., left vs. left) and of the opposite trial type (e.g., left vs. right). To do this comparison, we used an iterative procedure whereby we excluded one trial from the data set, calculated mean left and right firing rate vectors from the remaining trials, and then computed the standardized Euclidean distance between the excluded trial and the two means. Specificity was then computed as the difference between the two distances normalized by the total distance. Positive specificity values (i.e. activity was more similar to the same trial type) were considered accurate classifications. Classification accuracy for each training stage (Figure 2E; or behavioral performance, Figure 2H) was compared to a chance distribution calculated by shuffling trial type labels 10,000 times, and the observed classification accuracy was considered significant if it was greater than 97.5% of the control classification accuracies. To determine whether the observed classification accuracies differed between the four training stages, we shuffled individual neurons between stages 10,000 times, and then calculated the MSE of the four control classification accuracies after each shuffle. The observed MSE was considered statistically significant if it was greater than 97.5% of the shuffled MSEs.

**Reward location representations.**—We assessed the specificity of population firing at the reward locations in the same manner as the above analyses of population responses on the stem, by combining neurons from all subjects into a single population vector and computing the distance between firing rate vectors for right and left reward locations (Figure S2J). We compared the time window 1-3s after lick detection on left and right trials, as this was when the rats were most still and consuming the reward.

Decoding to Future Reward Areas.—Analyses of reward representations during stem traversals were similar to the above Bayesian analysis of spatial coding except that we sought to determine the degree to which the two reward locations were represented in the population activity rather than the rat's actual current position on the stem (Figures 3A–C). The analysis only included correct trials and the test sample was restricted to time bins as the rat traversed the stem. For each trial, we calculated the total decoded probability that the rat was in the reward areas. This included both instances of maximal decoding to the reward area and times when the firing patterns momentarily became more similar to the firing patterns observed when the rat was at the reward. Similar results were obtained when the analysis was limited to maximal classifications (Figures S2F and S2G). Reward areas included both the reward locations and the portion of the approach arms after the choice point (see boxes in Figure 3B). Most reward area decoding was at or near the reward locations, but some decoding was also seen along the arms. To determine whether the reward areas were overrepresented relative to other non-stem areas, we normalized the amount of decoding to the reward areas by their relative size (proportion decoding divided by proportion of pixels) and compared the observed value to chance (i.e. a uniform distribution, proportion of decoded probability is equal to proportion of total pixels; dotted line in Figure 3D). The statistical significance of each stage mean was calculated by comparing the observed distribution of session means to a value of one.

Representations of the two reward areas (left and right) were then compared to each other to determine whether the rat preferentially represented the correct reward area (Figure 3E). The difference between the representations (decoded probabilities) of the correct and incorrect reward areas were computed and then standardized by their sum (correct minus incorrect divided by the total). Positive values indicate a greater representation of the correct reward area, while negative values indicate a greater representation of the incorrect (previous) reward area. The statistical significance of each stage mean was calculated by comparing the observed distribution of session means to zero.

Assessment of Learning-Related Changes in Population Firing Patterns.—For all analyses involving neural populations recorded from individual rats (Figures 1E, 2B, 3D, and 3E), we evaluated the impact of training on firing patterns by fitting a linear mixed-effect model to the data with fixed effects for each training stage and uncorrelated random effects for intercept and training stage grouped by subject ('fitlme' in Matlab, Mathworks Inc.). We then tested whether this model was superior to a similar model that did not contain training stage predictors using an F-test ('coefTest' in Matlab).

#### DATA AND SOFTWARE AVAILABILITY

The data and analysis routines used in this study are available on request. Please contact the lead Contact, Adam M. P. Miller (amm473@cornell.edu)

# **Supplementary Material**

Refer to Web version on PubMed Central for supplementary material.

# Acknowledgements

We thank Sarah Parauda, Keunhyung Yu, Alexandra Tse, and Hui Jun Li for assistance with animal training and electrode microdrive fabrication. We thank Felix Thommes for assistance with the statistical analyses. We thank Howard Eichenbaum and A. David Redish for helpful comments on the manuscript. This work was supported by an NIH grant R01 MH083809 to D.M.S.

#### References

- 1. Corcoran KA, Donnan MD, Tronson NC, Guzman YF, Gao C, Jovasevic V, Guedea AL, and Radulovic J (2011). NMDA receptors in retrosplenial cortex are necessary for retrieval of recent and remote context fear memory. The Journal of neuroscience: the official journal of the Society for Neuroscience 31, 11655–11659. [PubMed: 21832195]
- Katche C, Dorman G, Gonzalez C, Kramar CP, Slipczuk L, Rossato JI, Cammarota M, and Medina JH (2013). On the role of retrosplenial cortex in long-lasting memory storage. Hippocampus 23, 295–302. [PubMed: 23355414]
- 3. Cowansage KK, Shuman T, Dillingham BC, Chang A, Golshani P, and Mayford M (2014). Direct reactivation of a coherent neocortical memory of context. Neuron 84, 432–441. [PubMed: 25308330]
- de Sousa AF, Cowansage KK, Zutshi I, Cardozo LM, Yoo EJ, Leutgeb S, and Mayford M (2019).
   Optogenetic reactivation of memory ensembles in the retrosplenial cortex induces systems consolidation
- Milczarek MM, Vann SD, and Sengpiel F (2018). Spatial Memory Engram in the Mouse Retrosplenial Cortex. Current biology: CB 28, 1975–1980.e1976. [PubMed: 29887312]

6. Ino T, Doi T, Hirose S, Kimura T, Ito J, and Fukuyama H (2007). Directional disorientation following left retrosplenial hemorrhage: a case report with fMRI studies. Cortex; a journal devoted to the study of the nervous system and behavior 43, 248–254. [PubMed: 17405670]

- 7. Pothuizen HH, Davies M, Aggleton JP, and Vann SD (2010). Effects of selective granular retrosplenial cortex lesions on spatial working memory in rats. Behavioural brain research 208, 566–575. [PubMed: 20074589]
- 8. Vann SD, and Aggleton JP (2002). Extensive cytotoxic lesions of the rat retrosplenial cortex reveal consistent deficits on tasks that tax allocentric spatial memory. Behavioral neuroscience 116, 85–94. [PubMed: 11895186]
- 9. van Groen T, and Wyss JM (1992). Connections of the retrosplenial dysgranular cortex in the rat. The Journal of comparative neurology 315, 200–216. [PubMed: 1545009]
- 10. van Groen T, and Wyss JM (2003). Connections of the retrosplenial granular b cortex in the rat. The Journal of comparative neurology 463, 249–263. [PubMed: 12820159]
- Brown TI, Carr VA, LaRocque KF, Favila SE, Gordon AM, Bowles B, Bailenson JN, and Wagner AD (2016). Prospective representation of navigational goals in the human hippocampus. Science (New York, N.Y.) 352, 1323–1326.
- 12. Cho J, and Sharp PE (2001). Head direction, place, and movement correlates for cells in the rat retrosplenial cortex. Behavioral neuroscience 115, 3–25. [PubMed: 11256450]
- Smith DM, Barredo J, and Mizumori SJ (2012). Complimentary roles of the hippocampus and retrosplenial cortex in behavioral context discrimination. Hippocampus 22, 1121–1133. [PubMed: 21630374]
- Chen LL, Lin LH, Green EJ, Barnes CA, and McNaughton BL (1994). Head-direction cells in the rat posterior cortex. I. Anatomical distribution and behavioral modulation. Experimental brain research 101, 8–23. [PubMed: 7843305]
- Jacob PY, Casali G, Spieser L, Page H, Overington D, and Jeffery K (2017). An independent, landmark-dominated head-direction signal in dysgranular retrosplenial cortex. Nature neuroscience 20, 173–175. [PubMed: 27991898]
- Vedder LC, Miller AM, Harrison MB, and Smith DM (2016). Retrosplenial Cortical Neurons Encode Navigational Cues, Trajectories and Reward Locations During Goal Directed Navigation. Cerebral cortex (New York, N.Y.: 1991).
- 17. Alexander AS, and Nitz DA (2015). Retrosplenial cortex maps the conjunction of internal and external spaces. Nature neuroscience 18, 1143–1151. [PubMed: 26147532]
- 18. Alexander AS, and Nitz DA (2017). Spatially Periodic Activation Patterns of Retrosplenial Cortex Encode Route Sub-spaces and Distance Traveled. Current Biology.
- 19. Vann SD, Aggleton JP, and Maguire EA (2009). What does the retrosplenial cortex do? Nature reviews. Neuroscience 10, 792–802. [PubMed: 19812579]
- 20. Mao D, Kandler S, McNaughton BL, and Bonin V (2017). Sparse orthogonal population representation of spatial context in the retrosplenial cortex. Nature communications 8, 243.
- 21. Zhang K, Ginzburg I, McNaughton BL, and Sejnowski TJ (1998). Interpreting neuronal population activity by reconstruction: unified framework with application to hippocampal place cells. Journal of neurophysiology 79, 1017–1044. [PubMed: 9463459]
- 22. Wilson MA, and McNaughton BL (1993). Dynamics of the hippocampal ensemble code for space. Science (New York, N.Y.) 261, 1055–1058.
- 23. Rigotti M, Barak O, Warden MR, Wang XJ, Daw ND, Miller EK, and Fusi S (2013). The importance of mixed selectivity in complex cognitive tasks. Nature 497, 585–590. [PubMed: 23685452]
- 24. Georgopoulos AP, and Carpenter AF (2015). Coding of movements in the motor cortex. Current opinion in neurobiology 33, 34–39. [PubMed: 25646932]
- 25. Wood ER, Dudchenko PA, Robitsek RJ, and Eichenbaum H (2000). Hippocampal neurons encode information about different types of memory episodes occurring in the same location. Neuron 27, 623–633. [PubMed: 11055443]
- Johnson A, and Redish AD (2007). Neural ensembles in CA3 transiently encode paths forward of the animal at a decision point. The Journal of neuroscience: the official journal of the Society for Neuroscience 27, 12176–12189. [PubMed: 17989284]

27. van der Meer MA, and Redish AD (2009). Covert Expectation-of-Reward in Rat Ventral Striatum at Decision Points. Frontiers in integrative neuroscience 3, 1. [PubMed: 19225578]

- 28. Bussey TJ, Muir JL, Everitt BJ, and Robbins TW (1996). Dissociable effects of anterior and posterior cingulate cortex lesions on the acquisition of a conditional visual discrimination: facilitation of early learning vs. impairment of late learning. Behavioural brain research 82, 45–56. [PubMed: 9021069]
- 29. Gabriel M (1993). Discriminative avoidance learning: a model system In Neurobiology of cingulate cortex and limbic thalamus. (Boston: Birkhauser), pp. 478–523.
- Czajkowski R, Jayaprakash B, Wiltgen B, Rogerson T, Guzman-Karlsson MC, Barth AL, Trachtenberg JT, and Silva AJ (2014). Encoding and storage of spatial information in the retrosplenial cortex. Proceedings of the National Academy of Sciences of the United States of America 111, 8661–8666. [PubMed: 24912150]
- 31. Frank LM, Brown EN, and Wilson M (2000). Trajectory encoding in the hippocampus and entorhinal cortex. Neuron 27, 169–178. [PubMed: 10939340]
- 32. Buckner RL, and Carroll DC (2007). Self-projection and the brain. Trends in cognitive sciences 11, 49–57. [PubMed: 17188554]
- 33. Schacter DL, Addis DR, Hassabis D, Martin VC, Spreng RN, and Szpunar KK (2012). The future of memory: remembering, imagining, and the brain. Neuron 76, 677–694. [PubMed: 23177955]
- 34. Kaplan R, King J, Koster R, Penny WD, Burgess N, and Friston KJ (2017). The Neural Representation of Prospective Choice during Spatial Planning and Decisions. 15, e1002588.
- 35. Ito HT, Zhang SJ, Witter MP, Moser EI, and Moser MB (2015). A prefrontal-thalamo-hippocampal circuit for goal-directed spatial navigation. Nature 522, 50–55. [PubMed: 26017312]
- 36. Pfeiffer BE, and Foster DJ (2013). Hippocampal place-cell sequences depict future paths to remembered goals. Nature 497, 74–79. [PubMed: 23594744]
- 37. Steiner AP, and Redish AD (2012). The road not taken: neural correlates of decision making in orbitofrontal cortex. Frontiers in neuroscience 6, 131. [PubMed: 22973189]
- 38. Redish AD (2016). Vicarious trial and error. Nature reviews. Neuroscience 17, 147–159. [PubMed: 26891625]
- 39. Lisman J, Buzsaki G, Eichenbaum H, Nadel L, Ranganath C, and Redish AD (2017). Viewpoints: how the hippocampus contributes to memory, navigation and cognition. Nature neuroscience 20, 1434–1447. [PubMed: 29073641]
- 40. Miller AMP, Vedder LC, Law LM, and Smith DM (2014). Cues, context, and long-term memory: the role of the retrosplenial cortex in spatial cognition. Frontiers in Human Neuroscience 8. [PubMed: 24478674]
- 41. McClelland JL, McNaughton BL, and O'Reilly RC (1995). Why there are complementary learning systems in the hippocampus and neocortex: insights from the successes and failures of connectionist models of learning and memory. Psychol Rev 102, 419–457. [PubMed: 7624455]
- 42. Katche C, Bekinschtein P, Slipczuk L, Goldin A, Izquierdo IA, Cammarota M, and Medina JH (2010). Delayed wave of c-Fos expression in the dorsal hippocampus involved specifically in persistence of long-term memory storage. Proceedings of the National Academy of Sciences of the United States of America 107, 349–354. [PubMed: 20018662]
- 43. Mao D, Neumann AR, Sun J, Bonin V, Mohajerani MH, and McNaughton BL (2018). Hippocampus-dependent emergence of spatial sequence coding in retrosplenial cortex. Proceedings of the National Academy of Sciences of the United States of America 115, 8015–8018. [PubMed: 30012620]
- 44. Remondes M, and Wilson MA (2015). Slow-gamma Rhythms Coordinate Cingulate Cortical Responses to Hippocampal Sharp-Wave Ripples during Wakefulness. Cell reports 13, 1327–1335. [PubMed: 26549454]
- 45. Paxinos G, and Watson C (1998). The rat brain in stereotaxic coordinates.
- 46. Olypher AV, Lansky P, Muller RU, and Fenton AA (2003). Quantifying location-specific information in the discharge of rat hippocampal place cells. Journal of neuroscience methods 127, 123–135. [PubMed: 12906942]
- 47. Markus EJ, Qin YL, Leonard B, Skaggs WE, McNaughton BL, and Barnes CA (1995). Interactions between location and task affect the spatial and directional firing of hippocampal

neurons. The Journal of neuroscience : the official journal of the Society for Neuroscience 15, 7079-7094. [PubMed: 7472463]

# Highlights

Retrosplenial (RSC) neural populations develop a spatial representation with learning

Late in learning, RSC activity can be used to predict future navigation decisions

After learning, the RSC simulates the correct future reward location

Lesions of the RSC selectively impair alternation performance after learning

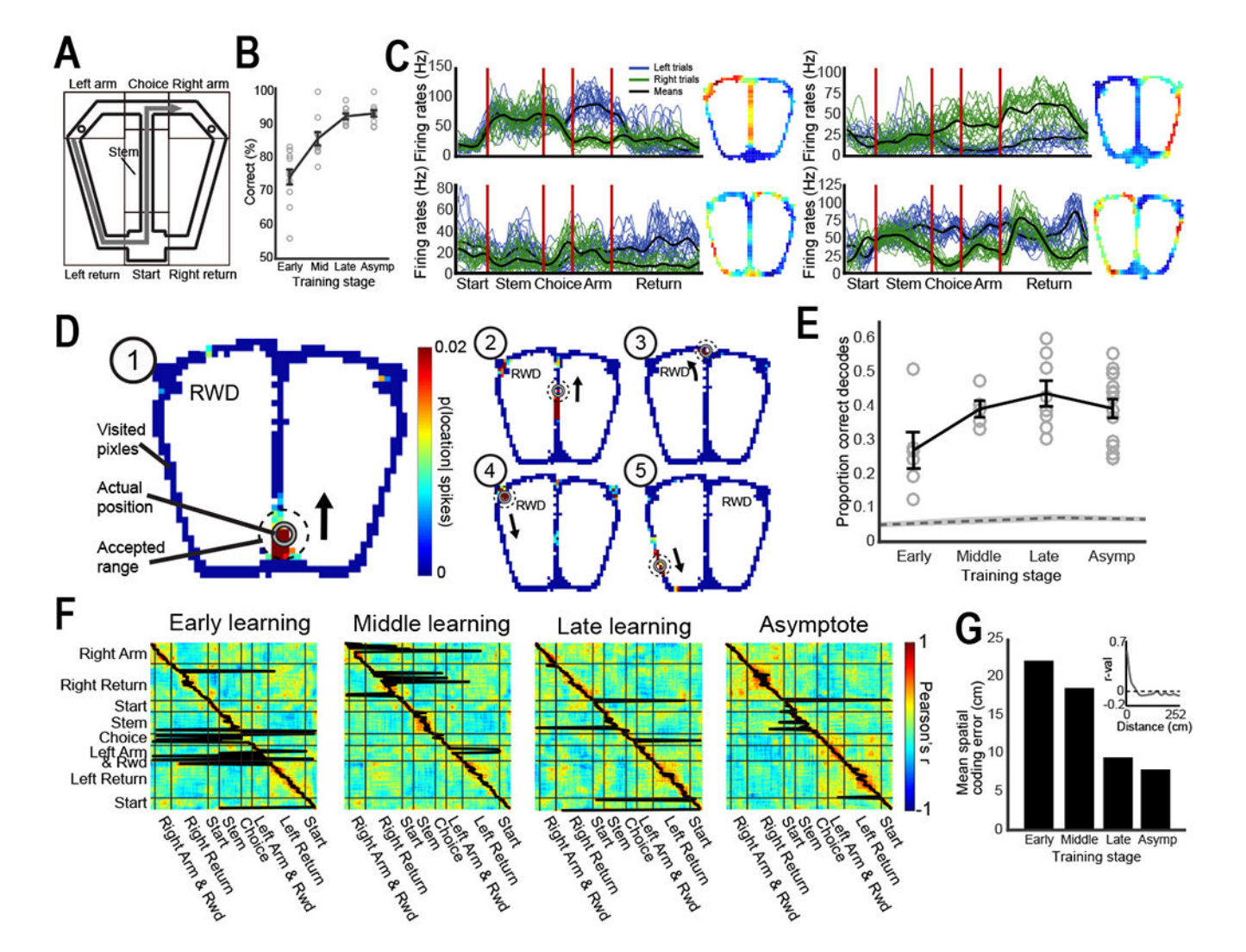


Figure 1. Neural populations in the retrosplenial cortex (RSC) developed a representation of the maze with learning.

(A) Schematic diagram of the continuous T-maze alternation task. After visiting one of the two reward locations (circles), rats returned to the stem and had to approach the opposite location for reward. (B) Behavioral performance across training stages, with average performance shown by the line plot (+/- SEM) and individual subjects indicated by circles. (C) RSC neuronal firing reliably distinguished maze regions. The firing of four example neurons illustrating the trial by trial firing as rats traversed the maze on left and right trials [17]. Red lines show maze section boundaries as depicted in a. Firing rate maps show the spatial distribution of firing rates for each example neuron. Neurons typically fired over large areas of the maze but differences in firing rates between spatial locations were quite reliable. (D) Bayesian decoding of the rat's current location on the basis of RSC population firing patterns. Five decoded instances from one trial are shown. Colors indicate the probability of the rat being in each pixel given the instantaneous spiking activity, with warmer colors corresponding to higher probabilities. The actual location of the rat's head is shown by the grey circle, and the rat's current direction of travel is indicated by the arrow.

Decoded locations (highest probability pixel) falling within the dashed circle (4.5 cm radius) were counted as correct. (E) RSC population encoding of spatial position improved with training. The decoder success rates for individual populations are plotted as open circles, with the mean indicated by the line. Decoding improved significantly with training and was always far more accurate than expected by chance (gray area shows the center 95% of the shuffle distribution). (F) Correlational analysis of RSC firing patterns also indicate that spatial representations improve with learning. A full lap around the maze was divided into 170 spatial bins (3 cm per bin) and correlation matrices were computed between firing rate vectors from the first and second half of each session at all spatial bins for each training stage. The black line connects the pixels of highest correlation between the two session halves at each spatial bin. Deviations from the diagonal indicate spatial coding errors. (G) Mean spatial coding error over all bins is plotted for each learning stage. Inset shows the mean population vector correlation for any two spatial locations as a function of the distance along the maze during asymptotic performance. Note that firing patterns from adjacent locations are well-correlated but the correlation decreases sharply with distance, indicating that population firing patterns are spatially specific. See also Figures S1–3.

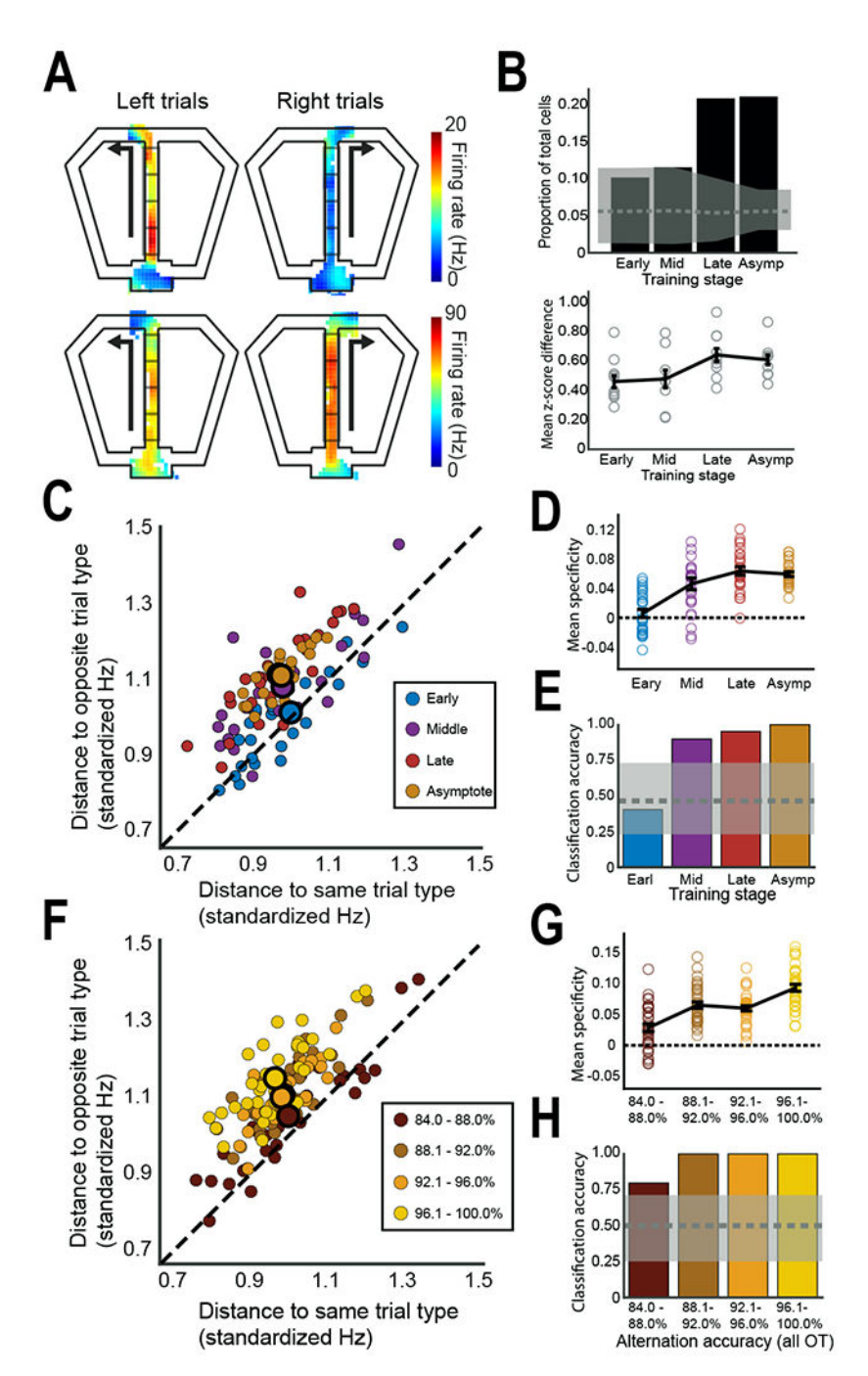


Figure 2. Neurons in the RSC develop trial-type specific firing on the stem.

(A) Two examples of RSC neurons (rows) that fired differently on the stem depending on whether the rat was about to turn left or right. Firing rate maps are shown for left and right turn trials, with the analyzed sectors of the stem indicated. (B) Top, the overall proportion of RSC neurons (from all subjects) showing trial-type specific firing is plotted across learning. Gray shading shows the chance (shuffled) mean and range for each stage. Bottom, trial-type specific firing is shown for each subject (circles) along with the mean (line). (C) Trial-type specificity of RSC population activity increased with training. Each colored dot shows

population activity from one trial (combined across subjects, see STAR Methods) plotted in terms of its distance from the mean of the same and opposite trial types. Points along the dotted line are equidistant to both trial types, indicating no preference for left or right trials, while points farther from the dotted line indicate stronger population preferences for one trial type over the other. Large dots outlined in black illustrate the mean for each learning stage (the Late mean is obscured). Note that population activity diverges from the unity line as learning progresses. (D) Trial-type specificity of the RSC population increased with training and was greater than chance by the middle training stage. Individual trials (small dots from C) are plotted as open circles, with the mean for each training stage illustrated by the line plot +/- SEM. (E) The ability to classify trials (left or right) solely on the basis of population firing patterns improved with learning, from chance (gray shading) early in learning, to perfect accuracy during asymptotic performance. (F-H) The trial-type specificity of RSC population firing was greater during sessions with better alternation performance. Plots are the same as C-E, except that all data were taken from asymptotic performance sessions that were grouped according to behavioral performance (% correct choices for the session). The mean of the 88.1-92.0% grouping is obscured. Note that population activity shows increased trial-type specificity and improved classification of left and right trials during sessions with superior behavioral performance. See also Figures S1 and S2.

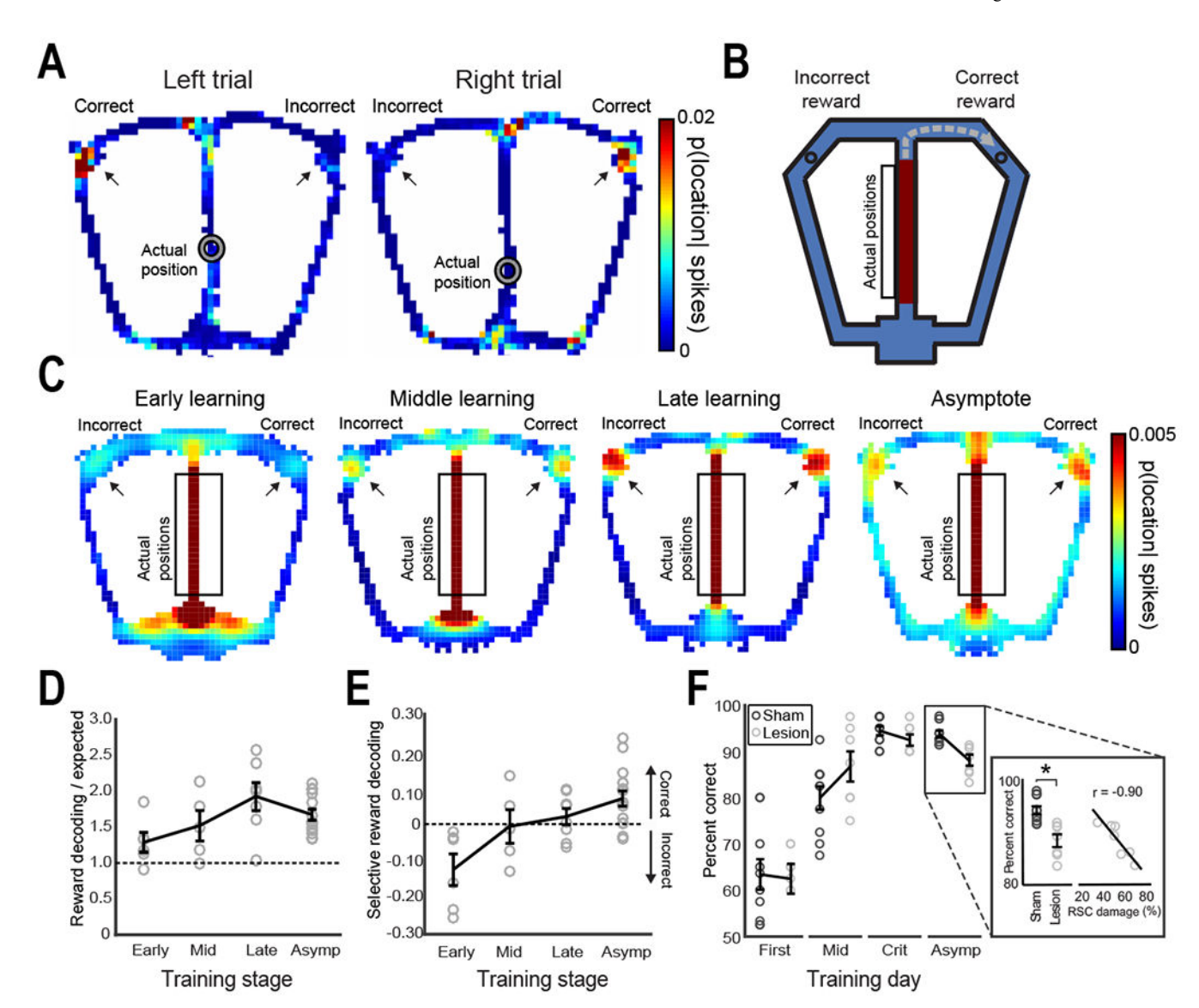


Figure 3. RSC populations represent upcoming reward locations.

(A) Bayesian decoding was used to identify representation of the upcoming reward locations (arrows) as rats approached the choice point. Two examples are shown, one left and one right trial, of decoded instances when population firing patterns were more consistent with the upcoming reward area than the rat's actual position (gray circle). (B) The analyses of decoded spatial information focused on the two reward locations and the distal part of the goal arms approaching each reward (black rectangles) but, importantly, was limited to time windows when the rat was located on the stem (red). (C) Heat maps illustrating the average decoded probability from all of the recorded populations from all of the rats, computed in 200 ms time bins as the rat traversed the stem, with separate heat maps shown for each learning stage. For illustration purposes, the data from the left trials are mirror reversed so that all the data are shown with the correct goal location to the right and the incorrect (previous) goal location shown to the left. Note the faint clouds of probability at the reward areas (i.e. decoding to the reward areas, arrows) during the early learning stage. This

becomes more prominent through late learning and only becomes selective for the correct reward area during asymptotic performance. Stem locations are uniformly red because the decoding is most prevalent at the rat's actual current location on the stem. (D) Decoding to the two reward areas increased with training and significantly exceeded chance levels (dashed line) only late in learning and during asymptotic performance. Individual populations are plotted as open circles, while average reward area decoding for each training stage is shown by the line plot +/- SEM. (E) Selective decoding to the correct reward area only became statistically significant during asymptotic performance. Future reward decoding was defined as the normalized difference between decoding to the correct reward area and the opposite (incorrect) reward area ((p(correct) – p(incorrect)) / p(correct) + p(incorrect)). Individual populations are plotted as open circles with the mean shown by the line plot. (F) Permanent lesions of the retrosplenial cortex selectively impaired spatial alternation performance after learning. Behavioral performance is plotted for the first (First), middle (Mid), and last (criterial, Crit) learning days, and asymptotic performance days (asymptotic performance, Aysmp). Performance for each control and lesion rat is shown as open circles, with the mean indicated by line plots. The inset illustrates asymptotic performance, along with the correlation between performance and lesion size. The inset illustrates asymptotic performance for control and lesion groups, and the lesion performance data plotted against lesion size. See also Figures S1–3.

# KEY RESOURCES TABLE

REAGENT or RESOURCE	SOURCE	IDENTIFIER
Experimental Models: Organisms/Strains		
Long-Evans rats	Charles River Laboratories	RGD Cat# 2308852, RRID:RGD_2308852
Software and Algorithms		
MATLAB	Mathworks	RRID: SCR_001622
SpikeSort3D	Neuralynx	RRID: SCR_014478
Other		
Digital Lynx Electrophysiology System	Neuralynx	Cat# 10SX-Z400 64 Ch System
Chocolate Milk	Nestle	n/a